Chapter 4

Results and Discussion

Characteristics of Hydroxyapatite

4.1 Characteristics of milled MP and TP powders.

a) Chemical analysis

The analyses of calcium, phosphorus and other impurities were carried out as summarised in the Table 4.1.   It was shown that both MP and TP had the same Ca:P ratio of 1.65 that was a little lower than the calculated stoichiometric one equivalent to 1.67.   The above results were due to the formation of calcium deficient hydroxyapatite.   Meanwhile the contamination of impurities in TP was decreased after chemical treatment compared to the original MP.

Table 4.1 Chemical composition of MP and TP powders.

composition	MP	TP
Ca (%)	38.7	38.8
P (%)	18.1	18.2
Ca:P	1.65:1	1.65:1
Impurities		
Mg (%)	0.616	0.464
Fe (ppm)	59.0	50.5
Zn (ppm)	168.5	33.0
Cu (ppm)	<1	<1
Mn (ppm)	<1	<1
Heavy metal		
Cd	<0.001	<0.001
Pb	<0.001	<0.001
Hg	<0.001	<0.001

b) Phase identification

From the patterns of the MP and TP powders determined by X-ray diffraction method as shown in Fig. 4.1. It was found that the phases of both powders were identified to be hydroxyapatite with the absence of the second phase. Apperently, the MP powder exhibited all sharp peaks implying a polycrystalline structure but the pattern of the TP really broad owing to incomplete crystallinity.
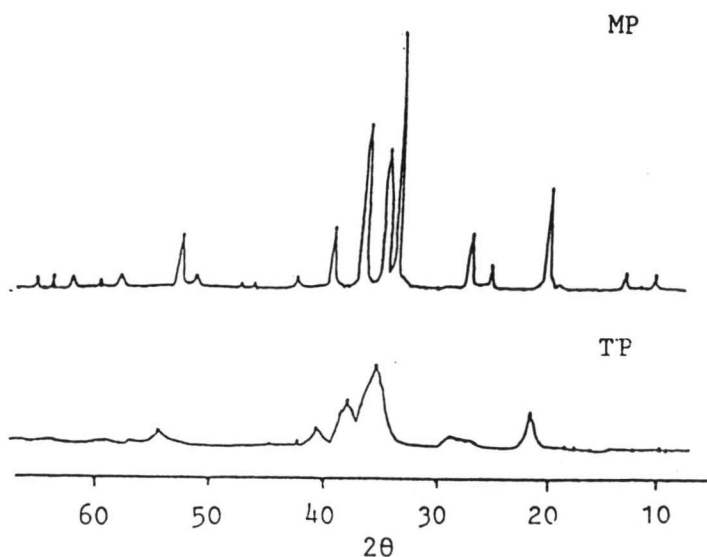

Figure 4.1 XRD patterns of MP and TP powders.

c) Microstructure and Particle size distribution

The microstructures of the MP and TP powders were illustrated in Fig. 4.2. It was indicated that the geometry of the MP and TP was similar with irregular agglomerate formation. But the MP particles were relatively larger than those of the TP.
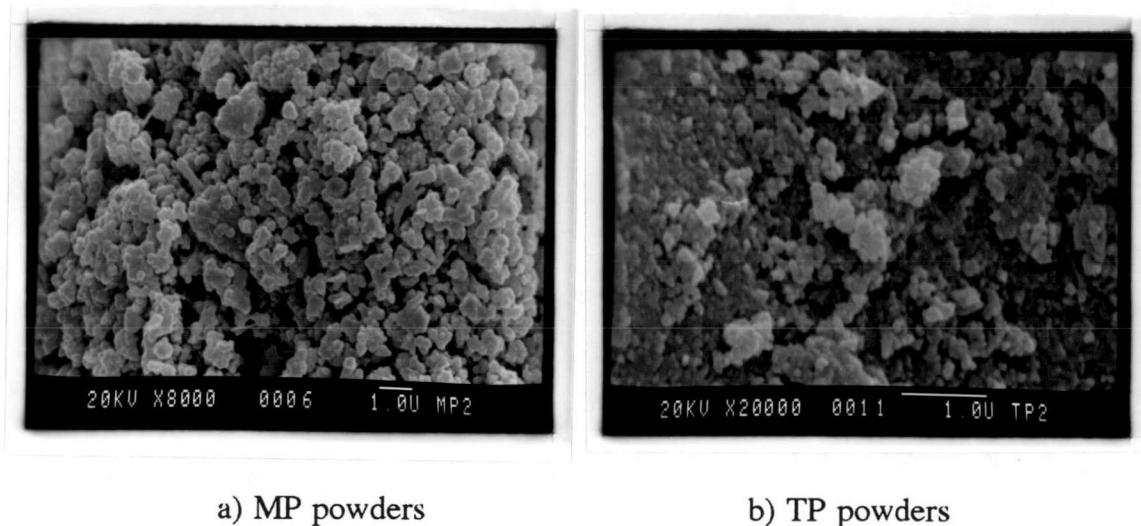

a) MP powders   b) TP powders

Figure 4.2 Scanning electron micrograph of MP and TP powders.

Particle size distribution of the MP and TP powders by sedimentation technique was shown in Fig. 4.3. It was seen that 80% of MP particle size was less than 2 μm but that of TP was less than 10 μm. The result contradicted against the value obtained from the micrograph (see Fig. 4.2) due to the formation of agglomerates in TP powder whose agglomerate of particle size was bigger than the actual value.
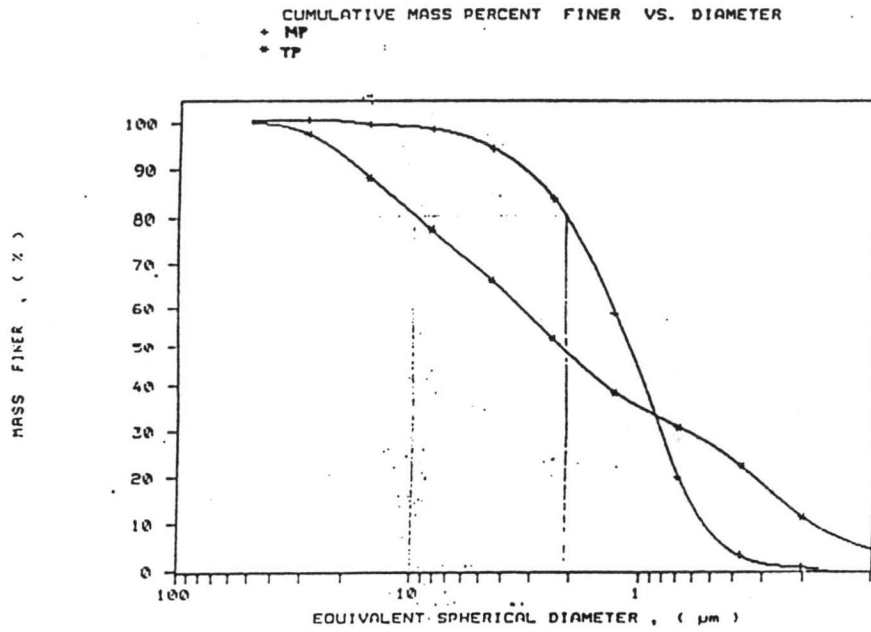
CUMULATIVE MASS PERCENT FINER VS. DIAMETER

Figure 4.3 Particle size distribution of MP and TP powders.

d) Density and Specific surface area

The density and specific surface area of the MP and TP powders were shown in Table 4.2.   The density of the TP was virtually lower than that of the MP due to the poor crystallinity and specific surface area of the TP is ten times larger as the result of the smaller particle size.

Table 4.2 Density and Specific surface area of MP and TP powders

Characteristics	MP	TP
Density (g/cm^3)	3.1341	2.9626
Specific surface area (m^2/g)	6.7474	67.5301

4.2 Characteristics of MP and TP granules

The characteristics of the MP and TP granules were shown in Table 4.3. It was seen that the ratio of tap density to filled density of the TP granules which showed the packing efficiency was slightly lower than that of the MP granules. However, the value of the TP was closer to one that was indicative of the denser packing in the mould.

Table 4.3 Characteristics of MP and TP granules.

Characteristics	MP	TP
Residue on # 35-50, %	90	90
Residue on # 50-140, %	10	10
Moisture, %	13.15	13.48
Filled density, g/cm^3	0.94	0.75
Tap density, g/cm^3	1.04	0.81
Tap density/ Filled density	1.11	1.08
Flow rate, g/sec	0.40	0.24

4.3 Characteristics of MP and TP compact bars

a) Compact density

The compact densities of the MP and TP compact bars were shown in Table 4.4.   It was indicated that the compact density of the TP was lower than that of MP due to the lower density of TP powder.
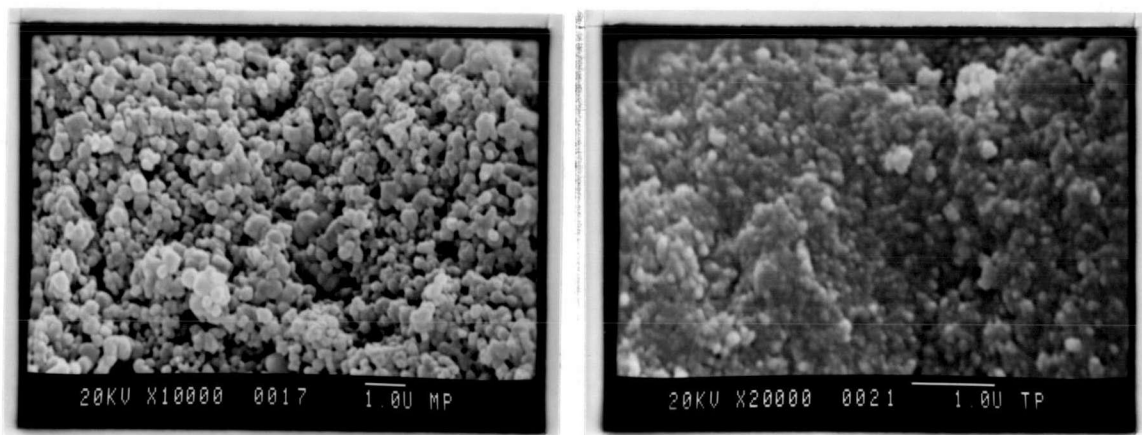
Table 4.4 Compact density of MP and TP compact bars.

Sample	Compact density (g/cm^3)
MP	1.95
TP	1.68

b) Microstructure

From the scanning electron microscope of the MP and TP compact bars as shown in Fig. 4.4. It was apperent that the agglomerates of the MP bar were loosely compact with larger void compared with those of the TP.

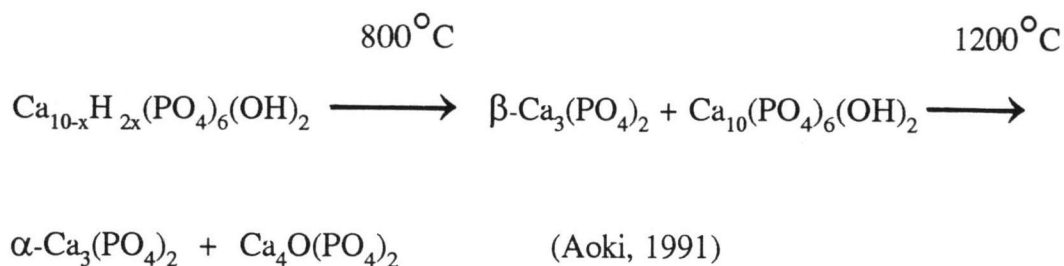

a) MP compact bar   b) TP compact bar

Figure 4.4 Scanning electron micrograph of MP and TP compact bars.

4.4 Characteristics of MP and TP sintered specimens

a) Phase identification

From the XRD patterns of the MP and TP sintered specimens as shown in Fig. 4.5 and 4.6 indicated that the phase of the sintered MP was only hydroxyapatite with the absence of the second phase at any sintering temperature whilst the sintered TP contained the presence of second phase of β-tricalcium phosphate. At the sintering temperature of 1200° and $1250^{\circ}C$, α-$Ca_3(PO_4)_2$ might be occurred but the α-$Ca_3(PO_4)_2$ was transformed to the β-$Ca_3(PO_4)_2$ when the product was cooled to room temperature in the furnace (Lorprayoon, 1986).

The occurrance of the second phase is subjected to thermal decomposition which takes place in accordance with the following non-stoichiometric equation as:
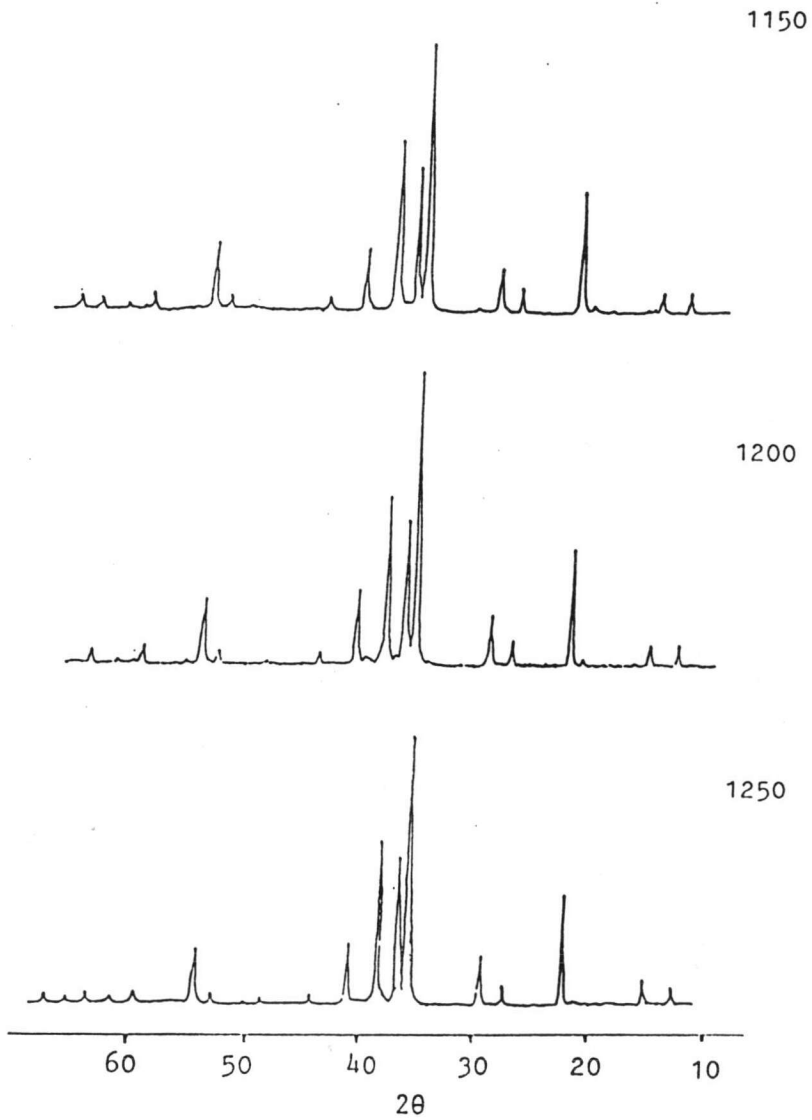
$$Ca_{10-x}H_{2x}(PO_4)_6(OH)_2 \xrightarrow{800^{\circ}C} \beta\text{-}Ca_3(PO_4)_2 + Ca_{10}(PO_4)_6(OH)_2 \xrightarrow{1200^{\circ}C}$$

$$\alpha\text{-}Ca_3(PO_4)_2 + Ca_4O(PO_4)_2 \qquad \text{(Aoki, 1991)}$$

1150

1200

1250

60 50 40 30 20 10

2θ

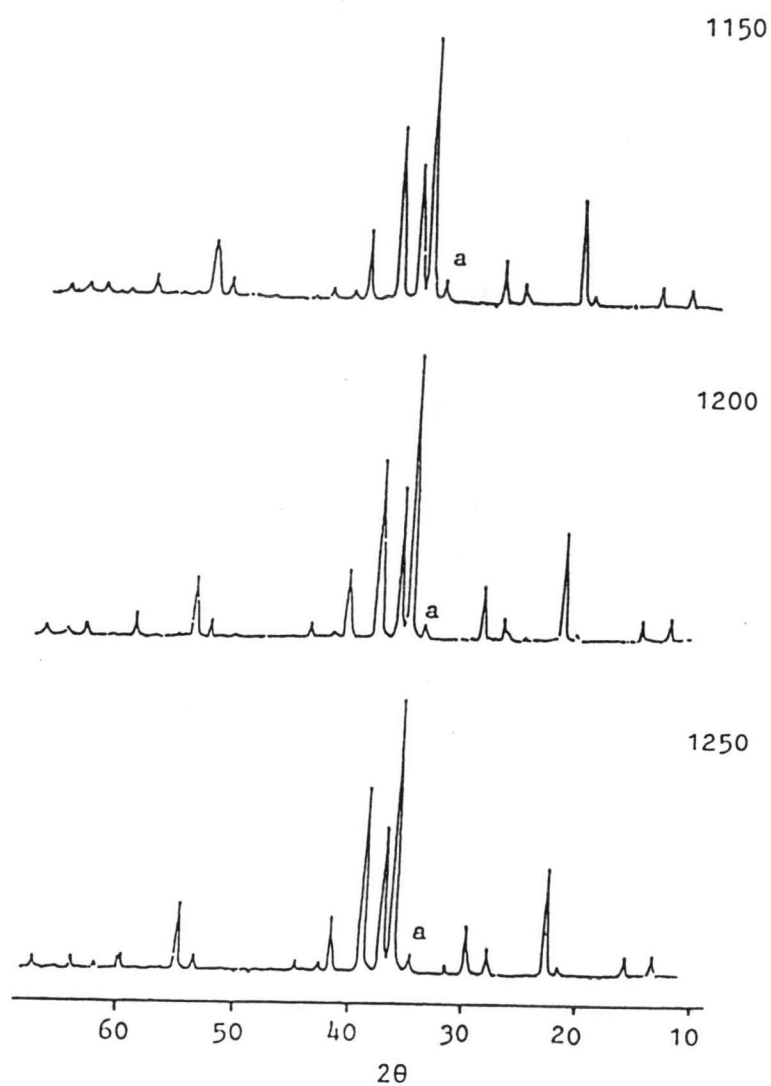Figure 4.5 XRD patterns of MP specimens sintered at 1150°, 1200° and
1250° C respectively.

Figure 4.6 XRD patterns of TP specimens sintered at 1150°, 1200° and

1250° C respectively.

a = β-tricalcium phosphate.

b) Microstructure

With respect to the scanning electron micrograph revealing the fracture surface of the MP and TP sintered specimens at different temperatures (1150° , 1200° and 1250° C respectively) as shown in Fig. 4.7. It was seen that the sintering of the TP was easily conducted at any temperature due to the greater specific surface area.   There is no significant increase in grain growth of the MP at higher sintering temperatures but only pore size is decreased.   However, the grain size of TP was found to increase at higher temperatures and excessive grain growth was observed due to the overfiring at 1250°C.   At the same sintering temperature, the grain size of MP was larger than that of the TP except at 1250°C.
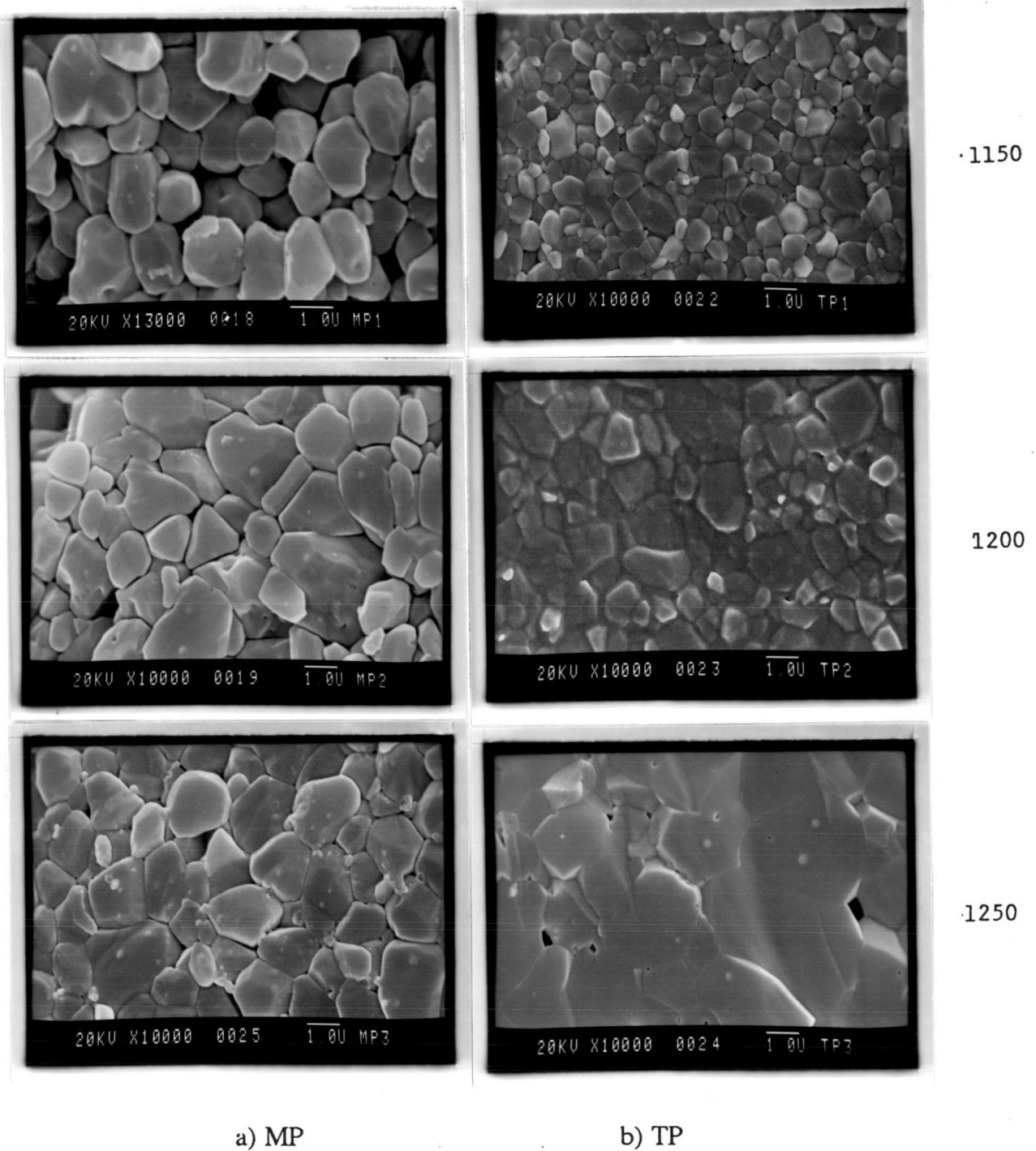
20KU X13000 0018 1.0U MP1

20KU X10000 0022 1.0U TP1

·1150

20KU X10000 0019 1.0U MP2

20KU X10000 0023 1.0U TP2

1200

20KU X10000 0025 1.0U MP3

20KU X10000 0024 1.0U TP3

·1250

a) MP   b) TP

Figure 4.7 Scanning electron micrograph of the MP and TP specimens sintered
at 1150°, 1200° and 1250° C respectively. (0.25% H_3PO_4 etching
for 15 sec).

c) Properties of MP and TP sintered specimens

The results of linear shrinkage, water absorption, apparent porosity, bulk density and relative density of the MP and TP specimens sintered at different temperatures (1150°, 1200° and 1250°C respectively) were shown in Table 4.5.   It was seen that the linear shrinkage, bulk density and relative density were increased at higher temperatures.   In contrast, water absorption and apparent porosity were found to be decreasing at higher temperatures. These resulted from the effects of pore shrinkage and grain growth during sintering process.   However, the TP showed superior properties to the MP due to the greater specific surface area of the TP which was easily sintered (Best, Bonfield and Doyle, 1989).   The relationships of linear shrinkage, water absorption, apparent porosity, bulk density and relative density versus sintering temperatures were shown in Fig. 4.8 -4.12 respectively.

Table 4.5 Properties of MP and TP sintered specimens.

Properties	Temperature(°C)	MP	TP
Shrinkage, %	1150	10.61	19.01
	1200	12.87	20.60
	1250	13.60	20.90
Water absorption, %	1150	4.13	0.69
	1200	0.62	0.42
	1250	0	0
Apparent porosity, %	1150	11.13	2.08
	1200	1.76	1.26
	1250	0	0
Bulk density, g/cm^3	1150	2.70	2.93
	1200	2.87	3.03
	1250	3.04	3.06
Relative density, %	1150	85.44	92.72
	1200	90.82	95.89
	1250	96.20	96.84
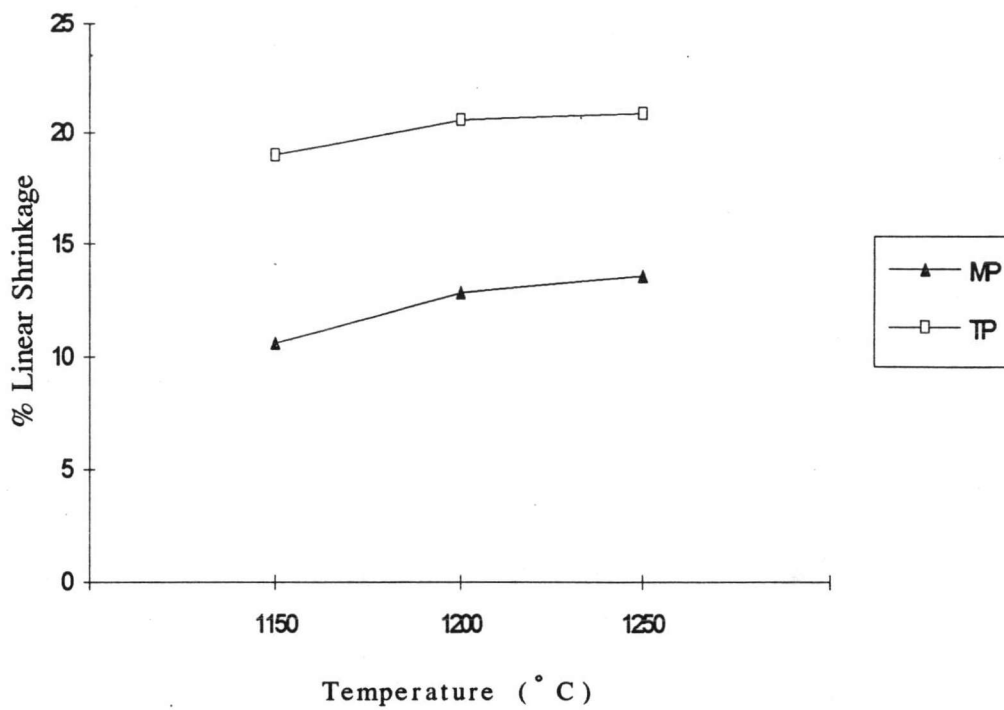
Figure 4.8 Linear shrinkage of MP and TP specimens sintered at 1150°,
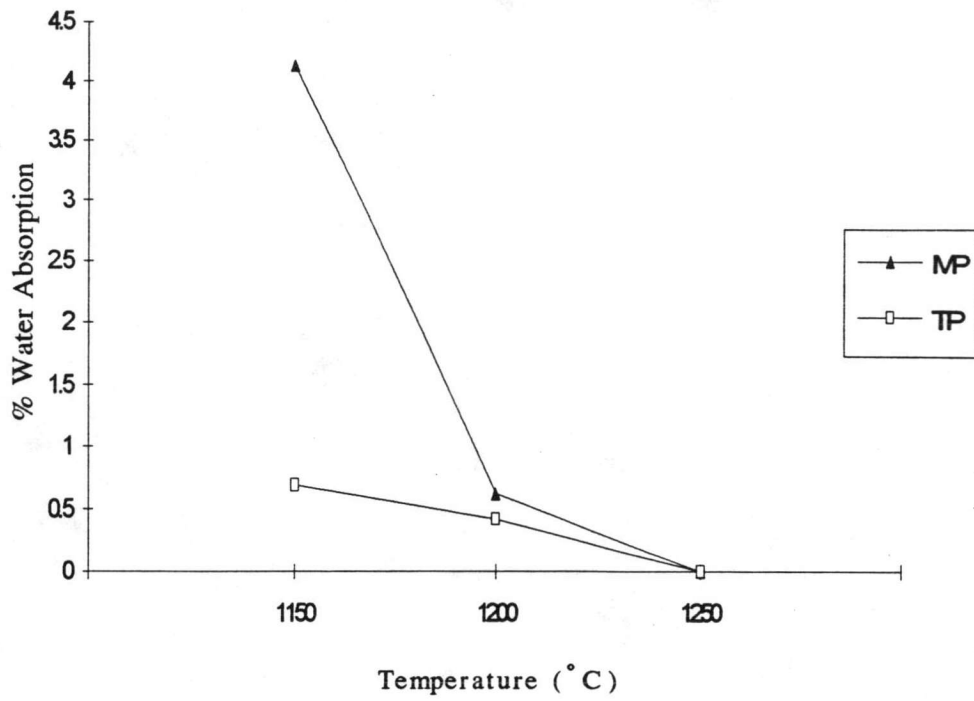
1200° and 1250°C respectively.

Figure 4.9 Water absorption of MP and TP specimens sintered at 1150°,
1200° and 1250°C respectively.
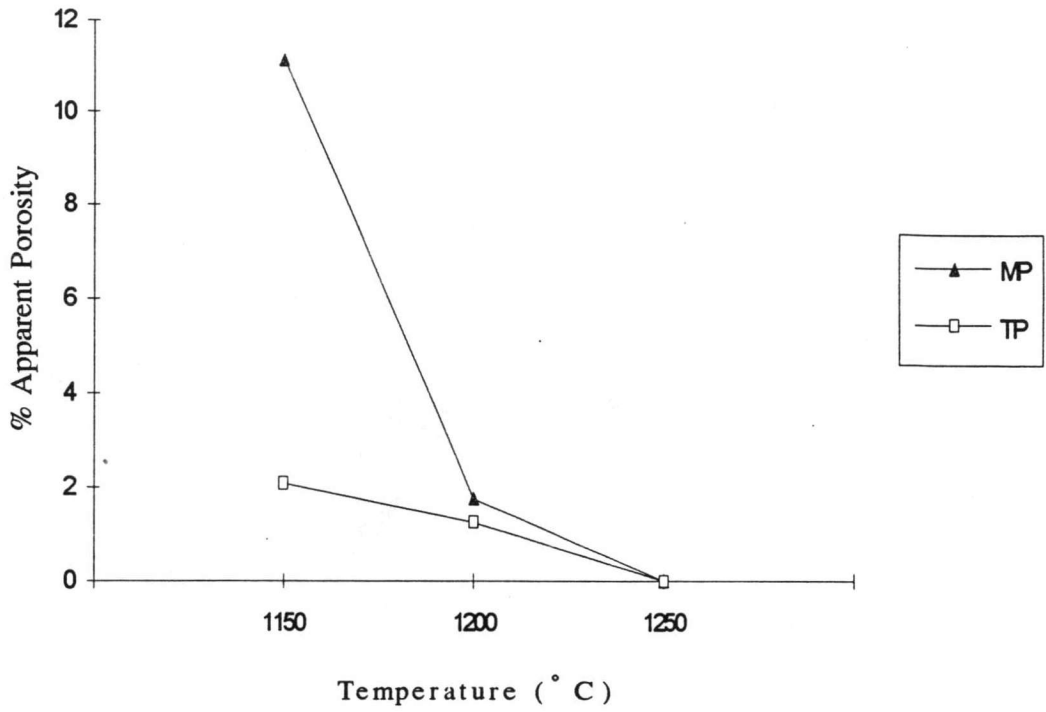
Figure 4.10 Apparent porosity of MP and TP specimens sintered at 1150°,

1200° and 1250°C respectively.
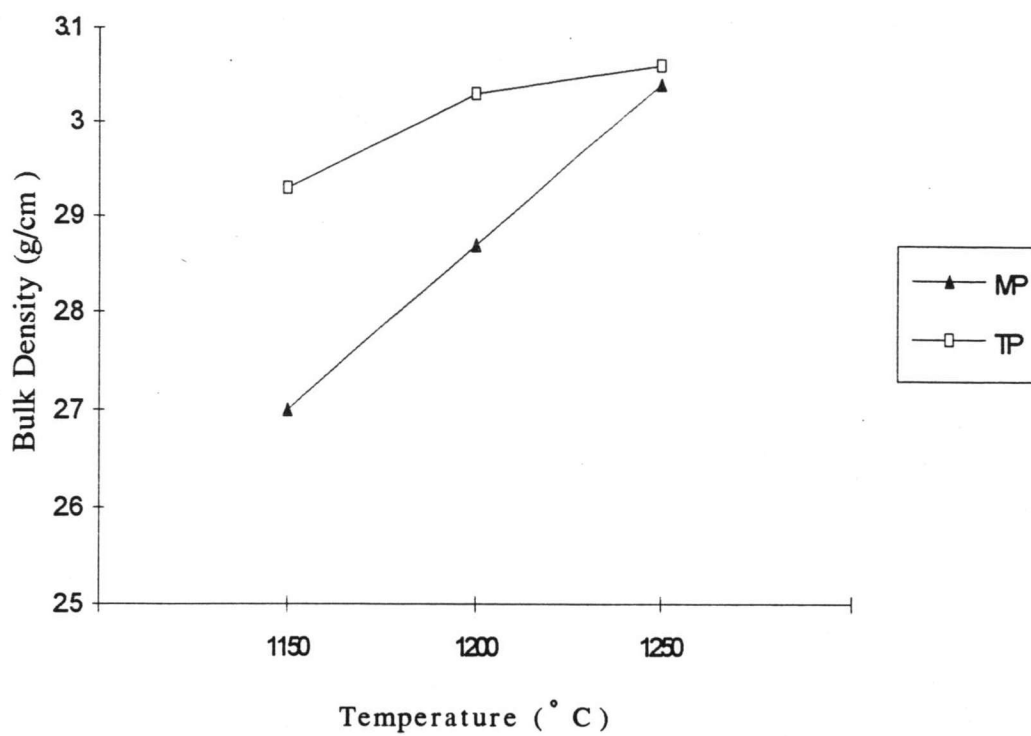
Figure 4.11 Bulk density of MP and TP specimens sintered at 1150°, 1200° and 1250°C respectively.
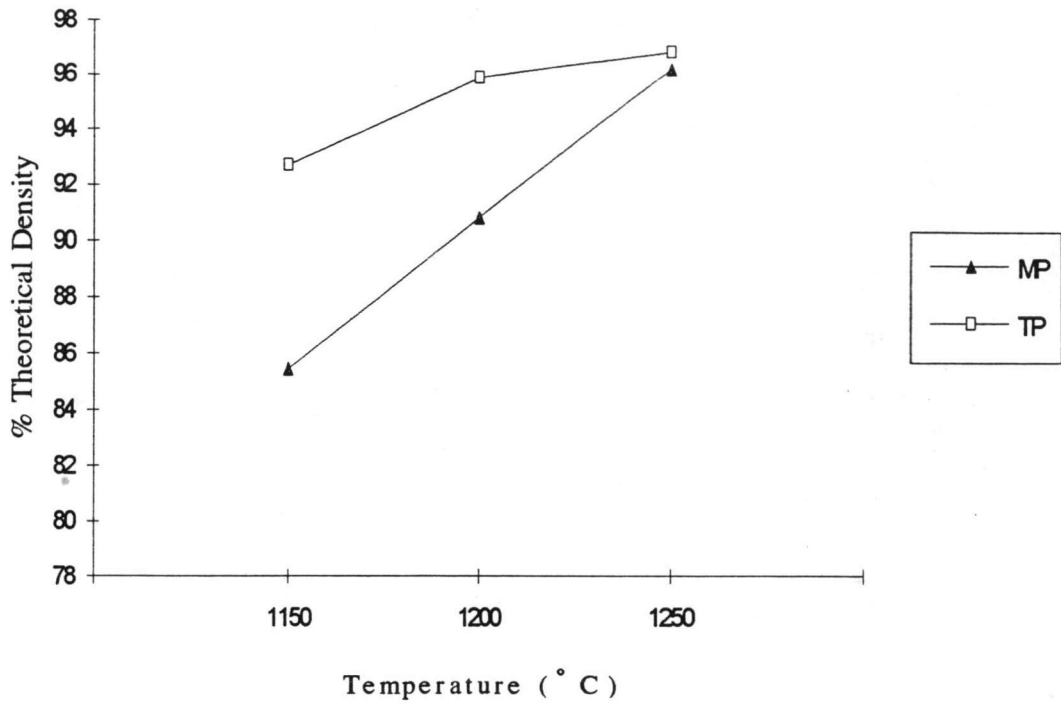
Figure 4.12 Relative density of MP and TP specimens sintered at 1150°, 1200° and 1250°C respectively.

d) Thermal expansion coefficient

The thermal expansion coefficients of the MP and TP specimens sintered at 1200°C were shown in Table 4.6.

Table 4.6 Thermal expansion coefficients of MP and TP specimens sintered at 1200°C.

Specimen	Thermal expansion coefficient at $(27\text{-}1200^\circ\text{C}) \times 10^{-6}$ K^{-1}
MP	14.12
TP	14.44

From the above result, the thermal expansion coefficient of the TP was slightly higher than that of the MP.

Mechanical Strength of Hydroxyapatite

The compressive strength of MP and TP specimens sintered at 1150°, 1200° and 1250°C respectively were shown in Table 4.7.

Table 4.7 Compressive strength of MP and TP sintered specimens.

Temperature($^\circ$C)	Compressive strength (MPa)	
	MP	TP
1150	157 ±23[*]	220 ±33[*]
1200	203 ±28[*]	291 ±29[*]
1250	245 ±43[*]	280 ±36[*]

[*] = standard deviation

It was found that the compressive strength of the MP and TP were rapidly increased at higher sintering temperatures except that of the TP at 1250°C as the result of the overfiring that induced the excessive grain growth as shown in Fig. 4.7.   The relationships of the compressive strength of the MP and TP versus sintering temperatures were shown in Fig. 4.13.

Nevertheless, the compressive strength of the TP is relatively higher than that of the MP because the TP is easily sintered and its grain is smaller compared to that of the MP (see Fig. 4.7).
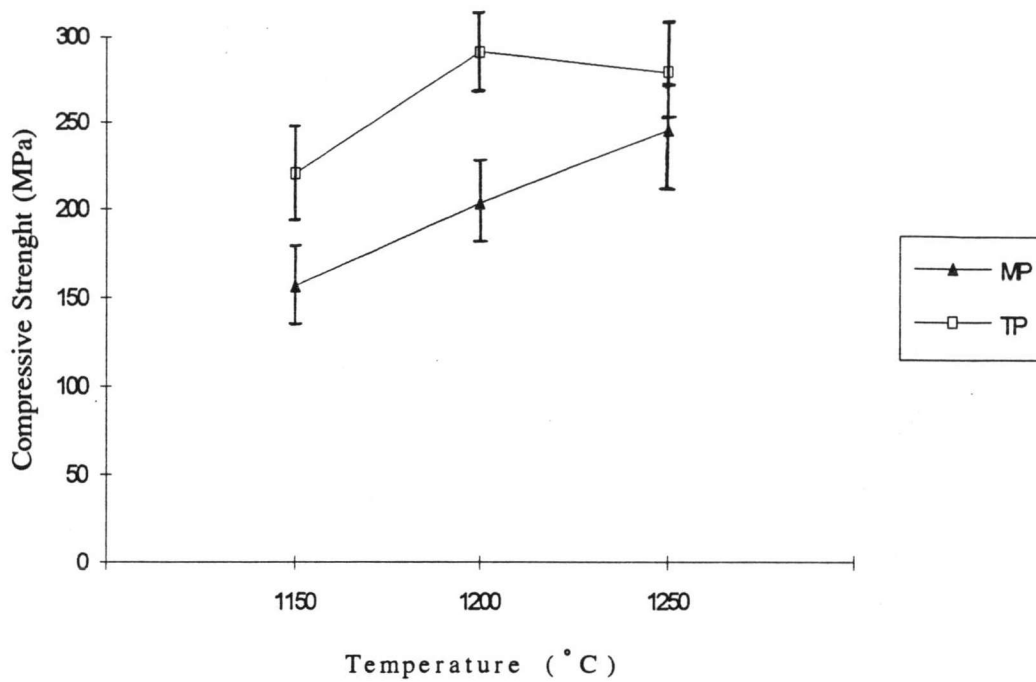
Figure 4.13 Compressive strength of MP and TP specimens sintered at 1150°, 1200° and 1250°C respectively.

Characteristics of Hydroxyapatite Mixtures

a) Compact density

The compact density of MPTP1-6 was obtained in Table 4.8.

Table 4.8 Compact density of MPTP1-6.

Specimen	Compact density, g/cm^3
MPTP1	1.95
MPTP2	1.94
MPTP3	1.93
MPTP4	1.85
MPTP5	1.78
MPTP6	1.75

It was indicated that the compact density of the MPTP1-6 was decreased when the proportion of the TP in the mixtures was higher due to the lower density of the TP.

b) Microstructure of compact bars

The microstructure of the compact bars of MP and TP mixtures as shown in Fig. 4.14 indicated that the agglomerates of the MP and TP mixtures were loosely compacted with large voids. This occurred because the inhomogenity of the mixtures was obtained and the TP particles were incapable of dispersing uniformly in the interstitial spaces between the MP agglomerates due to the limit in grain size. The packed density depends significantly on the form of the size distribution as well as the range of particle size. For the powder having a continuous size distribution, are blend in proportion that produce a continuous distribution that packs more densely. The size distribution of the blend is approximated by the Andreasen equation for dense packing

$$F_M(a) = \left[\frac{a}{a_{max}} \right]^n \qquad \text{cummulative quantity}$$

$$f_M(a) = \frac{n}{a} \left[\frac{a}{a_{max}} \right]^n \qquad \begin{array}{l} \text{differential quantity} \\ \partial F_M / \partial a = f_M \end{array}$$

where a_{max} is the maximum particle size and $1/n$ is the distribution modulus. In this model, the amount of a particular size in a constant fraction of the total amount finer than that size; i.e., the proportion of fine increases as the particle size decreases. Andreasen recognized that for a particular a_{max}, the porosity of the packed particle would decrease as n decreased; his experiments indicated that a practicle range of n was 0.33 and 0.50 (Reed, 1989).
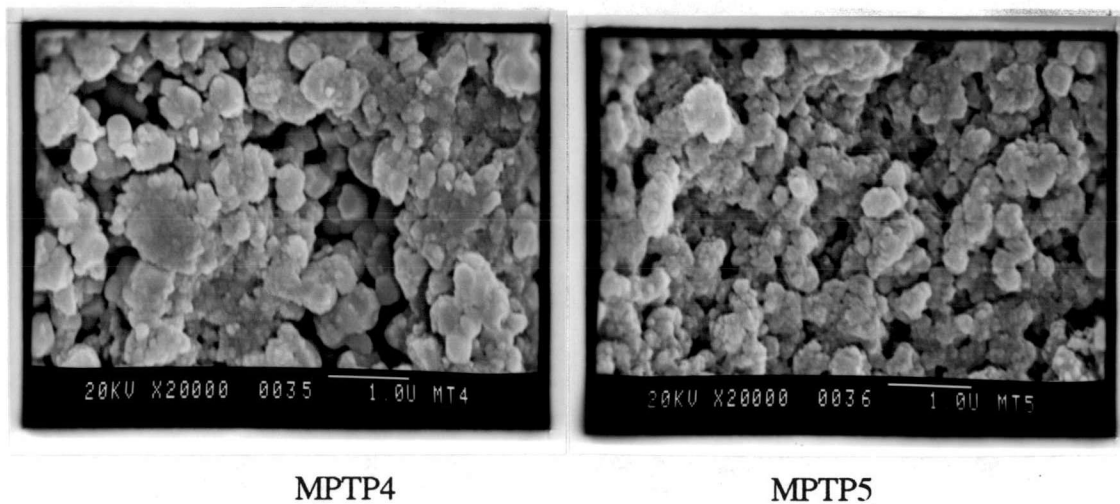
MPTP4   MPTP5

Figure 4.14 Scanning electron micrograph of MPTP4 and MPTP5 compact

bars.

c) Phase identification of MPTP1-6 sintered specimens

In the X-ray patterns, the specimens of MPTP1-6 sintered at 1200°C as shown in Fig. 4.15 . It was concluded that the phase of each specimen was identical to that of hydroxyapatite with the absence of the second phase.
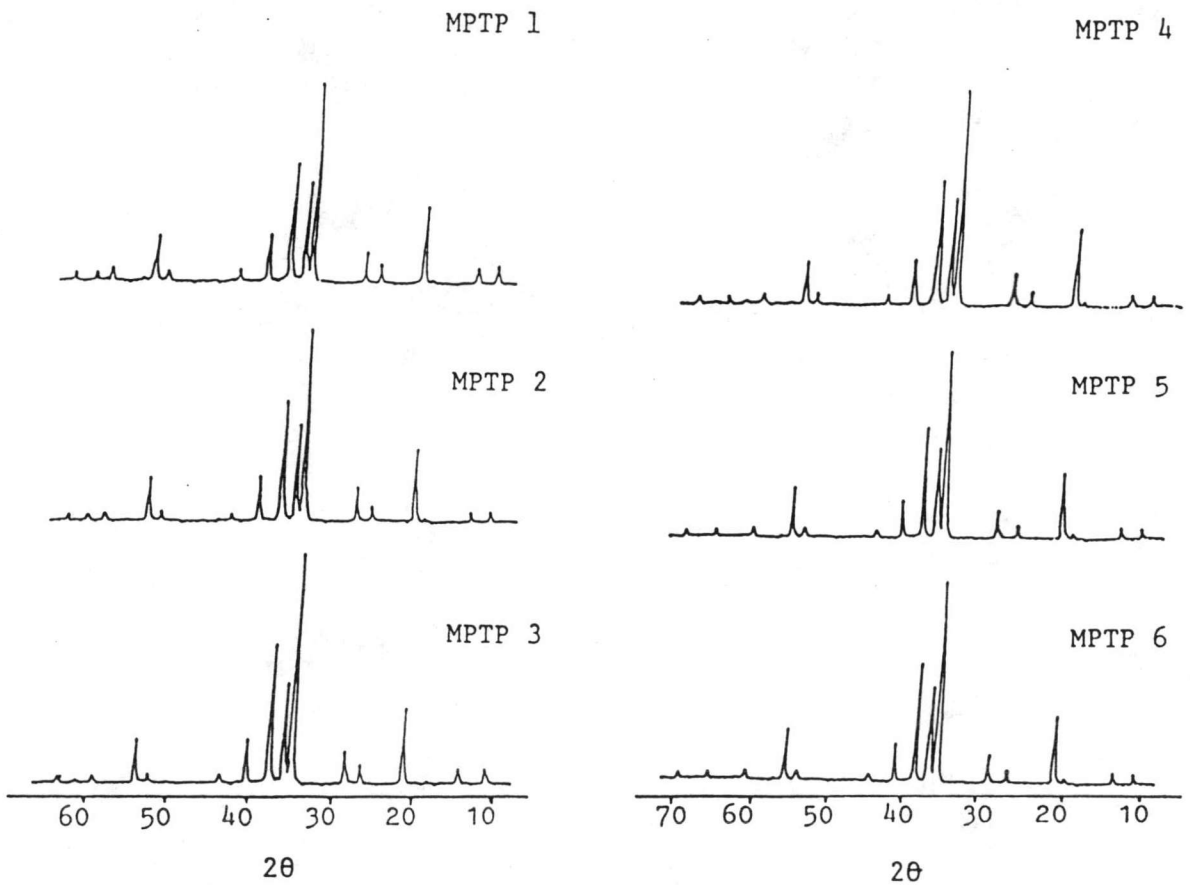

Figure 4.15 XRD patterns of MPTP1-6 sintered at 1200°C.

d) Microstructure of MPTP1-6 sintered specimens

With respect to scanning electron micrographs revealing the fracture surface of the specimens of MPTP1-6 sintered at 1200°C as shown in Fig. 4.16 , there were a number of voids in the mixtures as a result of loosely uniform dispersions of the TP particles that was easily sintered and contracted together to produce voids.
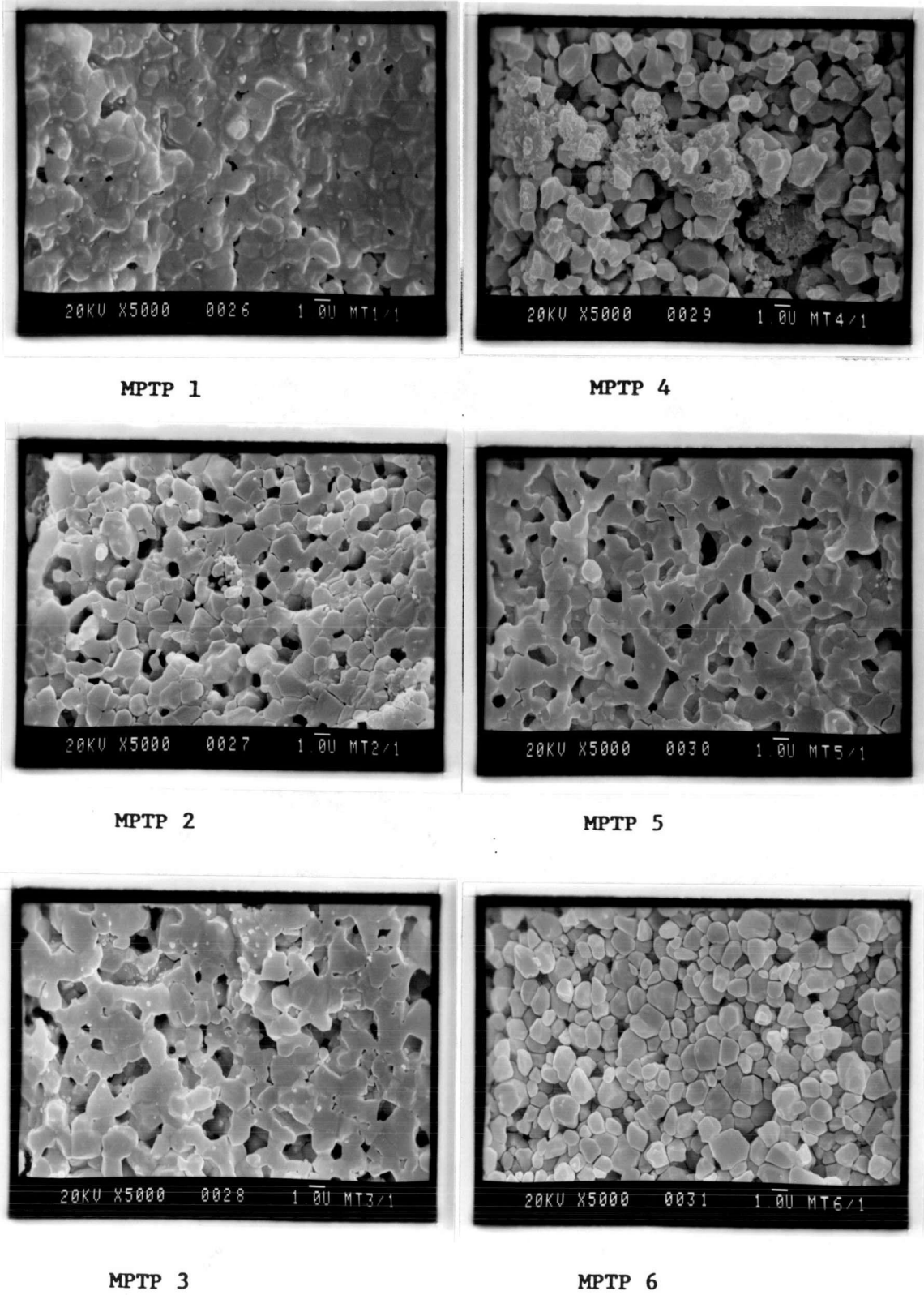
MPTP 1

MPTP 4

MPTP 2

MPTP 5

MPTP 3

MPTP 6

Figure 4.16 Scanning electron micrograph of MPTP1-6 sintered at 1200°C.

(0.25% H_3PO_4 etching for 15 sec)

e) Properties of MPTP1-6 sintered specimens

The change of linear shrinkage, water absorption, apparent porosity, bulk density and relative density of MPTP1-6 sintered at 1150°, 1200° and 1250°C respectively were observed in Table 4.9. It was pointed out that the linear shrinkage of MPTP1, 2 and 3 were closely inditical whereas MPTP4,5 and 6 containing 50% TP or more showed a increase in linear shrinkage at any sintering temperatures. On the contary, the water absorption and the apparent porosity were rapidly decreased when the proportion of TP was increased to 80% at any sintering temperatures. Similarly, the increase of bulk density and relative density were obtained when the proportion of TP is 80% higher. In comparison with the properties of MP and TP sintered specimens (see Table 4.8), these above results was considered unsatisfactory owing to loosely uniform microstructure of each mixture. The linear shrinkage, water absorption, apparent porosity ,bulk density and relative density of MPTP1-6 including those of MP and TP specimens sintered at 1150°,1200° and 1250°C were shown in Fig.4.17-4.21 respectively.

Table 4.9 Properties of MPTP1-6 sintered specimens

| Properties	Temp.($^{\circ}$C)	MPTP1	MPTP2	MPTP3	MPTP4	MPTP5	MPTP6
Shrinkage, %	1150	5.85	5.98	5.94	7.20	10.08	13.28
	1200	8.28	8.19	8.25	8.49	10.54	15.04
	1250	11.50	11.00	11.05	11.63	14.33	17.21
Water absorption, %	1150	9.27	10.91	11.67	11.50	10.89	6.15
	1200	5.91	6.36	7.48	8.18	8.18	2.04
	1250	1.06	1.27	2.81	3.72	2.71	0.26
Apperent porosity, %	1150	21.95	25.35	25.13	26.45	26.05	15.70
	1200	16.00	16.00	20.00	21.00	20.00	6.00
	1250	3.02	3.51	7.69	10.18	7.50	0.74
Bulk density, g/cm^3	1150	2.41	2.35	2.21	2.27	2.37	2.58
	1200	2.52	2.47	2.41	2.43	2.49	2.73
	1250	2.82	2.84	2.75	2.73	2.77	2.89
Relative density, %	1150	76.27	74.37	69.94	71.84	75.00	81.65
	1200	79.75	78.16	76.27	76.90	78.80	86.39
	1250	89.24	89.87	87.03	86.39	87.66	91.46
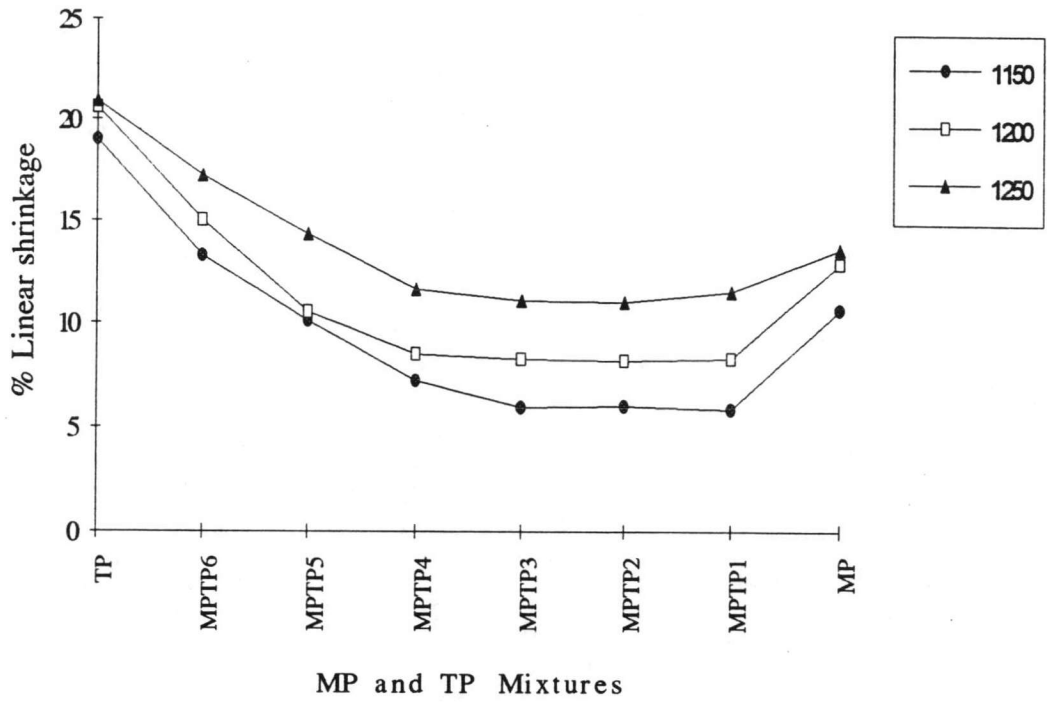
Figure 4.17 Linear shrinkage of MPTP1-6 including MP and TP specimens

sintered at 1150°, 1200° and 1250°C respectively.
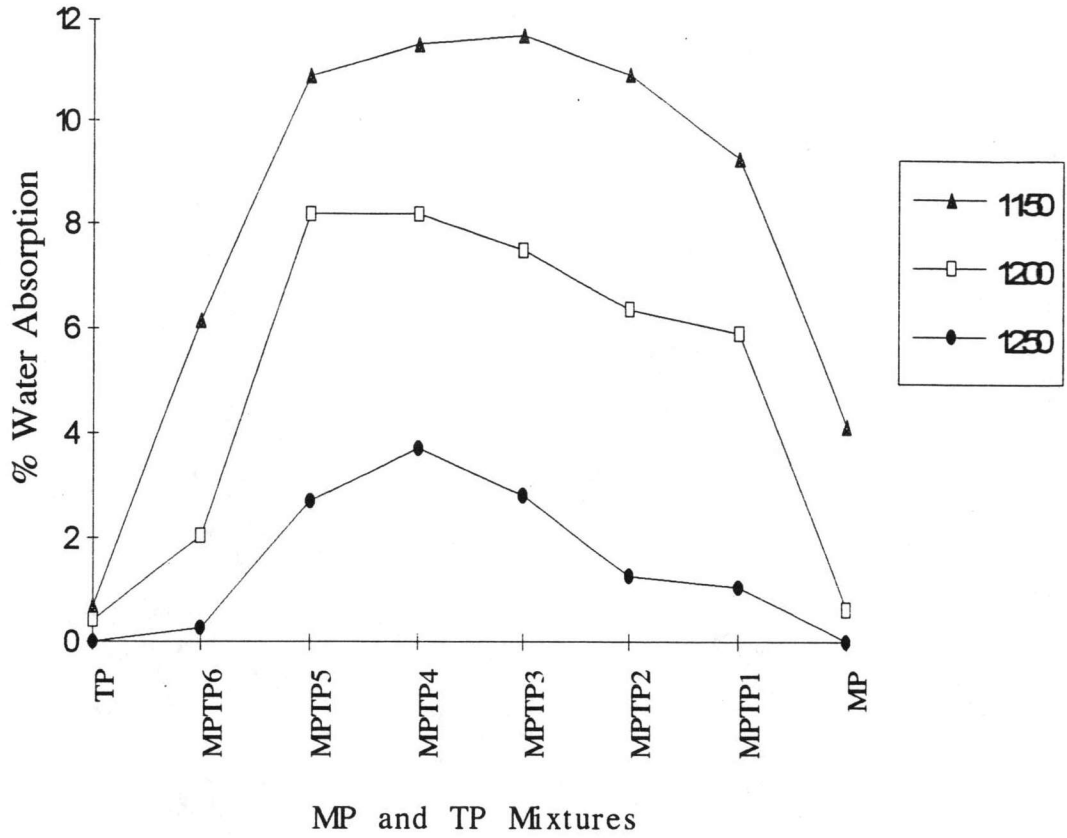
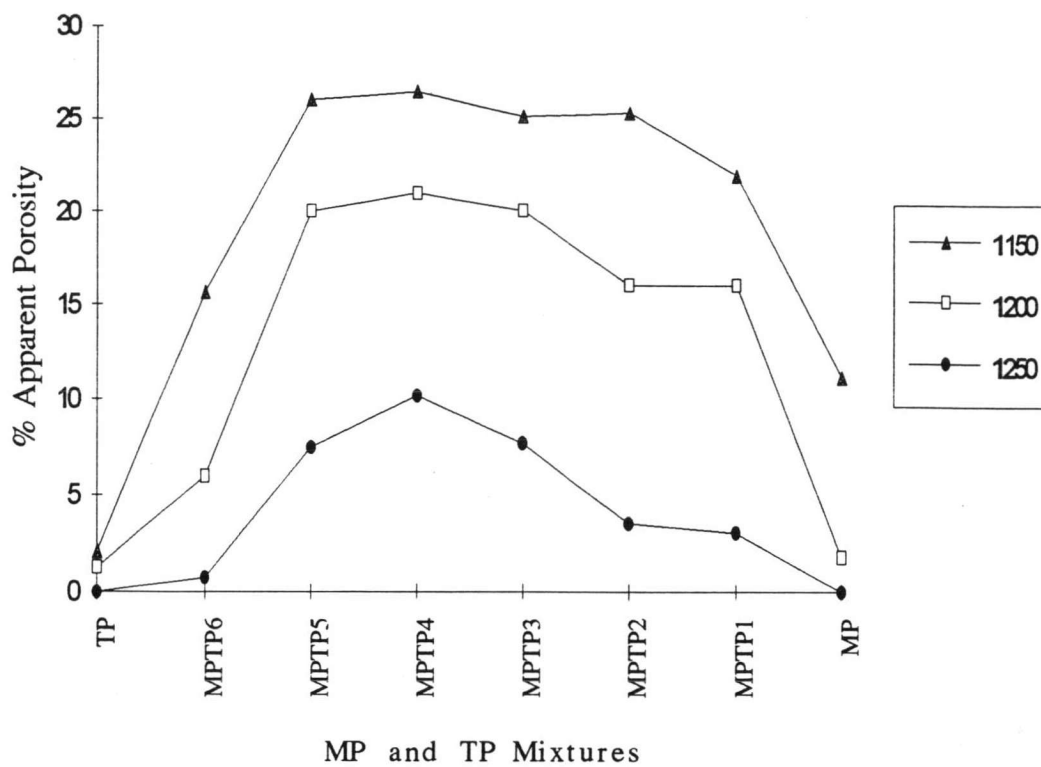Figure 4.18 Water absorption of MPTP1-6 including MP and TP specimens
sintered at 1150°,1200° and 1250°C respectively.

Figure 4.19 Apparent porosity of MPTP1-6 including MP and TP specimens
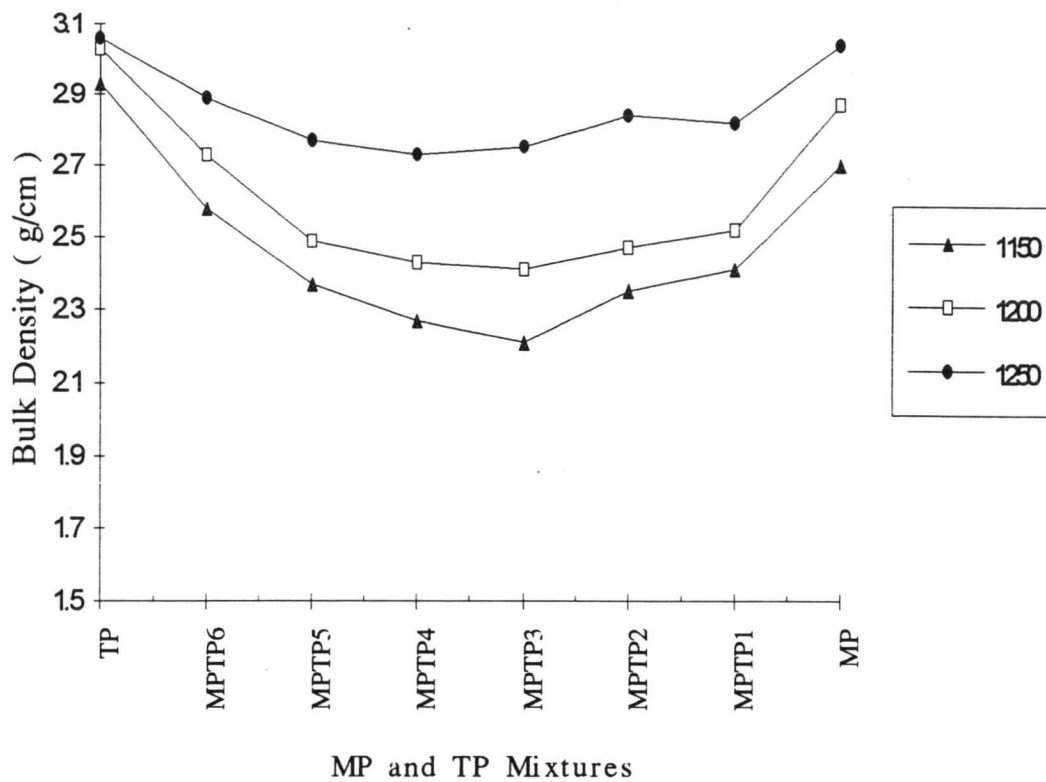
sintered at 1150°, 1200° and 1250°C respectively.

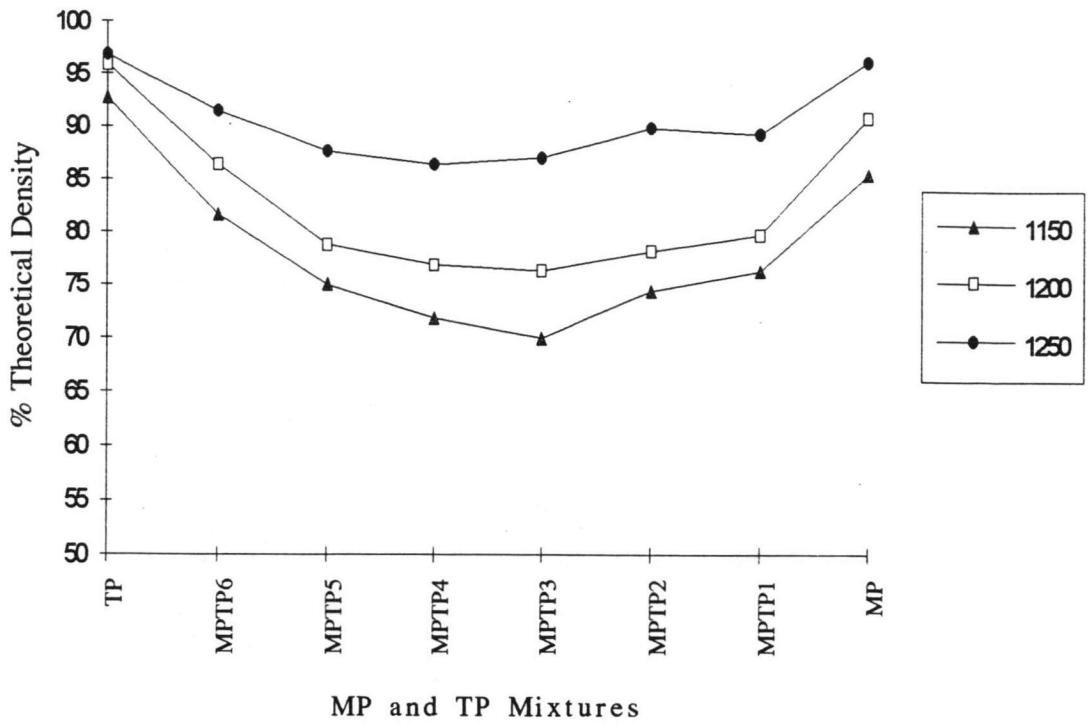Figure 4.20 Bulk density of MPTP1-6 including MP and TP specimens sintered at 1150°, 1200° and 1250°C respectively.

Figure 4.21 Relative density of MPTP1-6 including MP and TP specimens

sintered at 1150°, 1200° and 1250°C respectively.

e) Thermal expansion coefficient of MPTP1-6 sintered specimens

The thermal expansion coefficients of MPTP1-6 sintered at 1200°C were shown in Table 4.10.

Table 4.10 Thermal expansion coefficients of MPTP1-6 sintered at 1200°C.

Specimen	Thermal expansion coefficient at (27-1200°C)$\times$ 10^{-6} K^{-1}
MPTP1	14.47
MPTP2	14.46
MPTP3	14.49
MPTP4	14.50
MPTP5	14.18
MPTP6	14.25

The thermal expansion coefficients of MPTP1-4 were similar whereas those of MPTP5 and 6 were relatively smaller. In comparison with the results in Table 4.6, it was evident that the MP also showed a similar thermal expansion coefficient to MPTP5(14.12×10^{-6}K^{-1}). Considering the great difference in thermal expansion coefficient with that of TP(14.44×10^{-6}K^{-1}). The MP, MPTP5 and MPTP6 were therefore used as coating slips in the study.

Characteristics of Coated Hydroxyapatite

From the results of the compressive strength of MP and TP sintered specimens as shown in Table 4.7, the TP material therefore used as a body because the maximum strength was obtained at $1200^{\circ}C$.   Similarly, the material MP, MPTP5 and MPTP6 were selected as coatings slip due to the lower thermal expansion coefficient compared to that of the TP .

a) Thickness

The coating layer thickness of the coated TP specimen before sintering was measured by vernier caliper as shown in Table 4.11.

Table 4.11 Thickness of a coating layer of the coated TP.

Coated TP	Thickness (mm)
MP	0.23 ± 0.04
MPTP5	0.20 ± 0.04
MPTP6	0.26 ± 0.07

b) Phase identification of coated TP sintered specimens

From the XRD patterns of the TP specimen coated with MP, MPTP5 and MPTP6 and sintered at 1200°C as shown in Fig. 4.22.   It was indicated that all were indentified as the structure of hydroxyapatite with the second phase of β-tricalcium phosphate in minor quantities in contrast to that of the uncoated TP sintered at the same temperature.
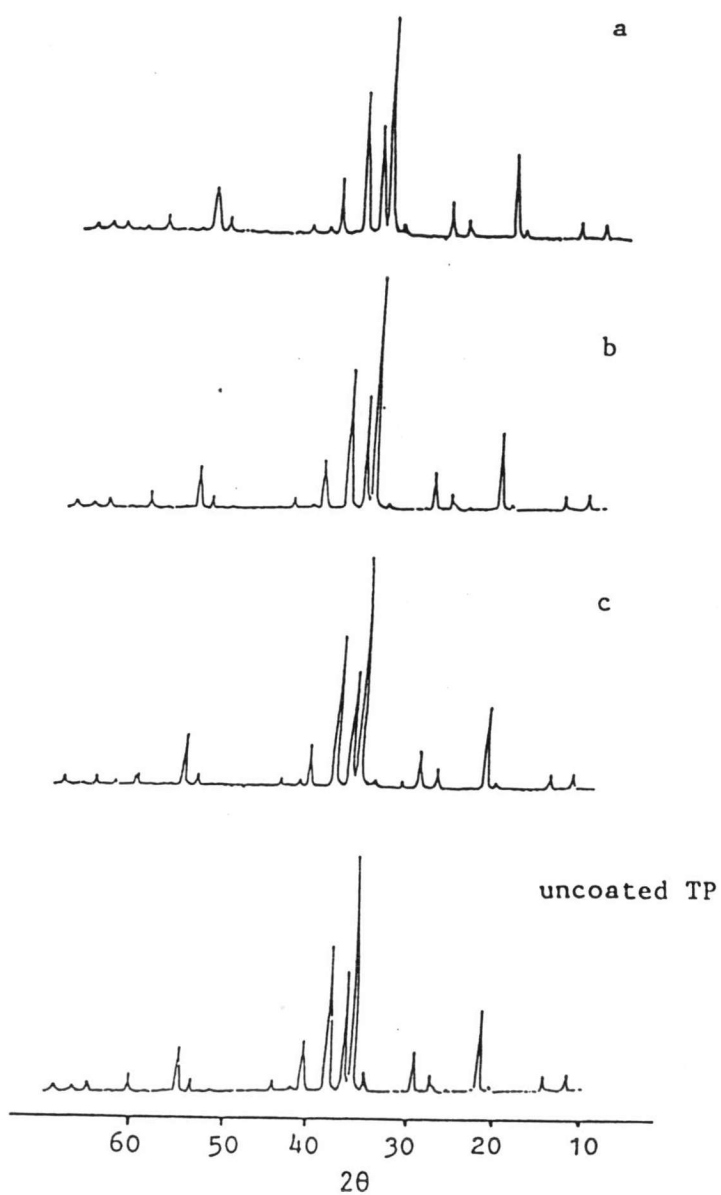
Figure 4.22 XRD patterns of coated TP with a) MP b) MPTP5 and c) MPTP6 after sintering at 1200°C.

c) Properties of coated TP sintered specimens

The results of water absorption, apparent porosity, bulk density and relative density of the TP specimens coated with MP, MPTP5 and MPTP6 sintered at 1200°C were shown in Table 4.12.   Apperently, the properties of the coated TP were found poorer than those of the uncoated one, in particular the water absorption and the apparent porosity increased.   On the other hand, the bulk density and relative density were shown to be decreasing substantially compared to those of the uncoated TP.   By the air spray method the coating produced a great number of pores on the surface, resulting in an increase in water absorption as well as porosity.

Table 4.12 Properties of coated TP specimens sintered at 1200°C.

| Properties	Uncoated TP	Coated TP		
		MP	MPTP5	MPTP6
Water absorption,%	0.42	3.40	3.64	3.52
Apparent porosity,%	1.26	10.00	10.00	10.50
Bulk density, g/cm^3	3.03	2.95	2.75	3.00
Relative density,%	95.89	93.35	87.03	94.49

d) Surface condition
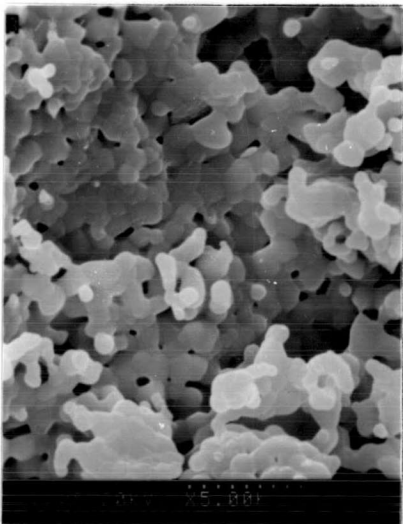
The surface conditions of a coating layer of the coated TP specimens sintered at 1200°C was determined by scanning electron microscopy as shown in Fig. 4.23. It was observed that there was a great number of pores scattering on the surface of the coating layer compared to the uncoated one.
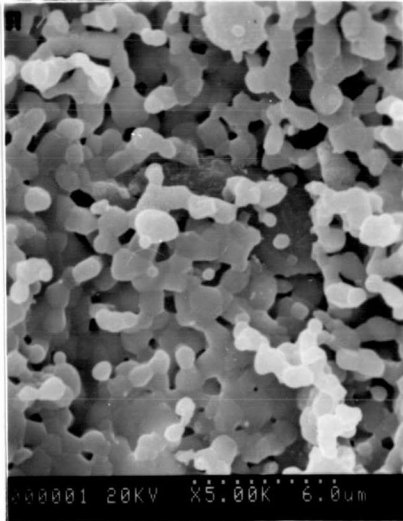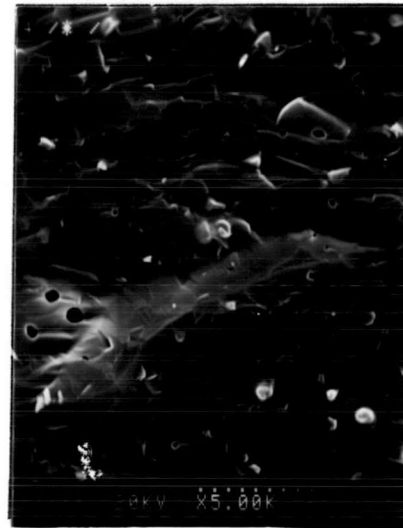

a
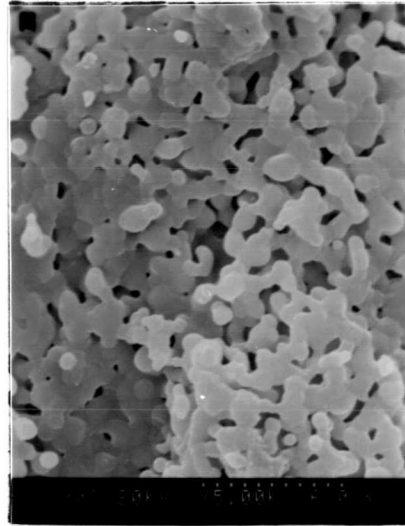
b

c

uncoated TP

Figure 4.23 Surface condition of coated TP with a) MP b) MPTP5 and c) MPTP6 sintered at 1200°C.

Mechanical Strength of Coated Hydroxyapatite

The compressive strength of the coated TP using coating slips of MP, MPTP5 and MPTP6 respectively sintered at 1200°C were shown in Table 4.13

Table 4.13 Compressive strength of the coated TP with MP, MPTP5 and MPTP6 sintered at 1200°C.

Coated TP	Compressive strength (MPa)
MP	$218 \pm 36^*$
MPTP5	$212 \pm 32^*$
MPTP6	$234 \pm 35^*$

* = standard deviation

As seen in Table 4.7 and Fig. 4.13, the TP specimen was shown to have the compressive strength of 291 ± 29 MPa. Unfortunately, the strengthening of the coated TP was lower than to the uncoated one when MP, MPTP5 and MPTP6 were used as the coating slips. It was seen that the compressive strength of the TP coated with MP, MPTP5 and MPTP6 were decreased to 25%, 27% and 19.6% respectively. All results might be attributed to the following factors:

1. The difference in thermal expansion coefficient between the body and the coating was too small. In fact, the TP has value of $14.44 \times 10^{-6} K^{-1}$ but those of MP, MPTP5 and MPTP6 are $14.12 \times 10^{-6} K^{-1}$, $14.25 \times 10^{-6} K^{-1}$ and 14.18

$\times 10^{-6} K^{-1}$ respectively. Each coating has the difference of only 2.1%, 1.3% and 1.8% respectively compared to the TP. From the work of Kirchner et al. (1968) using 96% Al_3O_2 body having the thermal expansion coefficient of 6.5 $\times 10^{-6} K^{-1}$ coated with a glaze having the thermal expansion coefficient of $5.3 \times 10^{-6} K^{-1}$. It has been found that the strength of the body having the difference in thermal expansion coefficient to 18.46% is increased to 40% as the result of the induced compressive surface stresses. Similarly, the work of Moody(1969) involving the coating of a TiC body having the thermal expansion coefficient of $8.0 \times 10^{-6} K^{-1}$ with B_4C having that of $5.6 \times 10^{-6} K^{-1}$, it has been proved that there is an increase in the strength up to 50% with the difference in thermal expansion coefficient of 30%. In addition, Kirchner et al. (1971) used a zircon porcelain with the thermal expansion coefficient of $2.6 \times 10^{-6} K^{-1}$ glazed with CVD-Si_3N_4 having that of $4.1 \times 10^{-6} K^{-1}$, it has been proved that the strength is raised up to 40% with the difference in thermal expansion coeffient of 36%. In comparison with the above results, indeed, there is no compressive surface stresses to be induced in the coated TP.

2. The different process of forming, by which the TP body was obtained by hydraulic pressing but the coating was performed by air spraying method that resulted in the formation of pores on the surface (see Fig. 4.23). Subsequently, the relative density of the coated TP decreased when compared to the uncoated one (see Table 4.12). This result would effect a significant decrease in compressive strength as shown in Fig. 4.24 (Richerson, 1982).
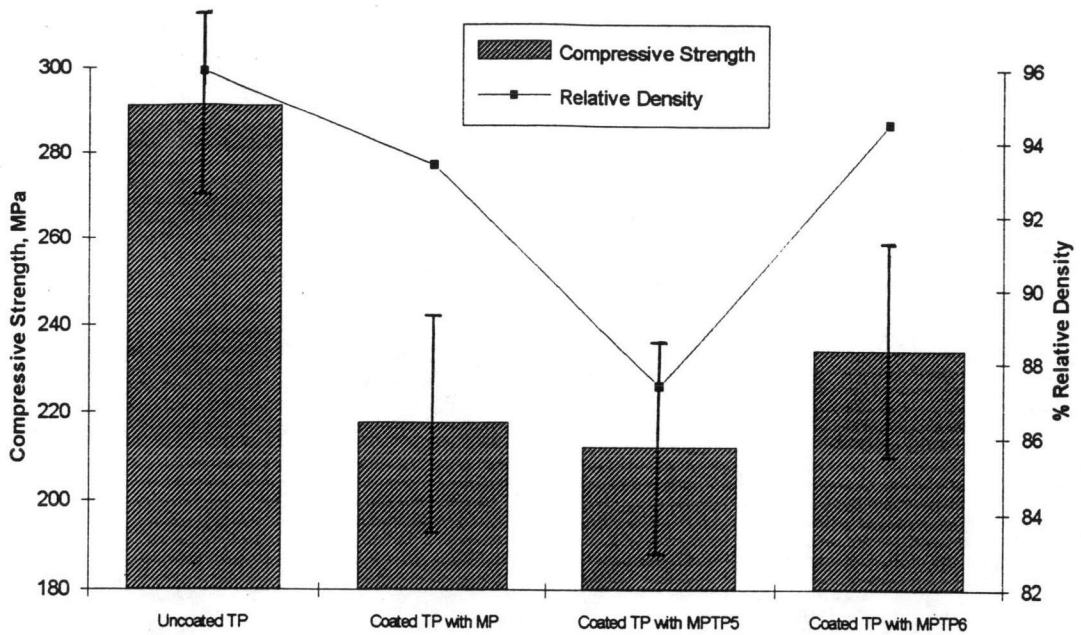
Fig. 4.24 The relationship of compressive strength and relative density of
uncoated and coated TP with MP, MPTP5 and MPTP6.

From the Griffith equation (Kingery et al., 1991) as follows:

$$\sigma = \left(\frac{Er}{c} \right)^{1/2}$$

where σ = Strength

E = Young modulus

r = Surface energy

c = Crack length

The occurrence of pores in the coating is similar to the phenomenum of
cracking, causing the strength lower.

3. The occurrence of β-tricalcium phosphate in the TP coated with MP, MPTP5 and MPTP6 was smaller than that in the uncoated TP because the abundance of TCP showed a significant increase in the strength of mixed HAp-TCP ceramics. (Aoki, 1991).

4. The great contrast in linear shrinkage between the body and the coating layer , in other words, the linear shrinkage of the TP body was 20.60% while those of MP, MPTP5 and MPTP6 were 12.87%, 10.54% and 15.04% respectively leading to the breakdown of the attraction between the body and its surface of the coating surface during cooling.

The above results might be possible to lower the strength of coated TP compared to that of uncoated one.